PAPER

A Monte Carlo study for the calculation of the average linear energy transfer (LET) distributions for a clinical proton beam line and a radiobiological carbon ion beam line

To cite this article: F Romano *et al* 2014 *Phys. Med. Biol.* **59** 2863

IOP Publishing | Institute of Physics and Engineering in Medicine Physics in Medicine and Biology

Phys. Med. Biol. **59** (2014) 2863–2882 doi:10.1088/0031-9155/59/12/2863

A Monte Carlo study for the calculation of the average linear energy transfer (LET) distributions for a clinical proton beam line and a radiobiological carbon ion beam line

F Romano[1], G A P Cirrone[1], G Cuttone[1], F Di Rosa[2], S E Mazzaglia[1], I Petrovic[3], A Ristic Fira[3] and A Varisano[1]

[1] INFN-Laboratori Nazionali del Sud, Via S. Sofia, 62 - I-95123 Catania, Italy
[2] Azienda Provinciale Sanitaria di Caltanissetta, Via G. Cusmano, 1 - I-93100 Caltanissetta, Italy
[3] University of Belgrade, Vinca Institute of Nuclear Sciences, P.O. Box 522, 11001 Belgrade, Serbia

E-mail: francesco.romano@lns.infn.it

Received 7 January 2014, revised 24 March 2014
Accepted for publication 23 April 2014
Published 14 May 2014

Abstract

Fluence, depth absorbed dose and linear energy transfer (LET) distributions of proton and carbon ion beams have been investigated using the Monte Carlo code Geant4 (GEometry ANd Tracking). An open source application was developed with the aim to simulate two typical transport beam lines, one used for ocular therapy and cell irradiations with protons and the other for cell irradiations with carbon ions. This tool allows evaluation of the primary and total dose averaged LET and predict their spatial distribution in voxelized or sliced geometries. In order to reproduce the LET distributions in a realistic way, and also the secondary particles' contributions due to nuclear interactions were considered in the computations. Pristine and spread-out Bragg peaks were taken into account both for proton and carbon ion beams, with the maximum energy of 62 MeV/n. Depth dose distributions were compared with experimental data, showing good agreement. Primary and total LET distributions were analysed in order to study the influence of contributions of secondary particles in regions at different depths. A non-negligible influence of high-LET components was found in the entrance channel for proton beams, determining the total dose averaged LET by the factor 3 higher than the primary one. A completely different situation was obtained for carbon ions. In this case, secondary particles mainly contributed in the tail that is after the peak. The results showed how the weight of light and heavy secondary ions can considerably influence the computation of LET depth distributions. This has an important role in

the interpretation of results coming from radiobiological experiments and, therefore, in hadron treatment planning procedures.

Keywords: hadrontherapy, Monte Carlo simulation, linear energy transfer, biological effect, Bragg peak

1. Introduction

Over the last few years there has been growing interest in the use of light ions for therapeutic purposes. Synergistic effects of ballistic precision and high biological efficiency make hadrontherapy with light ions more advantageous with respect to conventional radiotherapy with photon beams (Paganetti and Kooy 2010, Baumert *et al* 2001, Brada *et al* 2007, Kraft 2000, Schardt *et al* 2010). So far, more than 90 000 patients have been treated worldwide with protons and about 10 000 with carbon ions (PTCOG). Although physical characteristics of these beams are widely known, predictions of the biological damage and the consequent cellular response still need to be improved (Wambersie 1999). In hadrontherapy, the quantitative estimation of the biological effect is commonly given by using the concept of relative biological effectiveness (RBE): it is defined as the ratio of the absorbed dose of the reference radiation, such as ^{60}Co gamma rays, and the dose given by the specific radiation type which produces the same biological effect. The latter is most frequently quantitatively measured by means of the cell survival fraction. RBE usually varies for different positions inside the target volume and it depends on various kinds of parameters such as: cell line, surviving fraction, dose, ion species and, in particular, the linear energy transfer (LET) (Belli *et al* 1998, Wouters *et al* 1996, Gerweck and Kozin 1999, Paganetti and Gotein 2001). Different particle species for the same LET value produce distinct biological effects, i.e., RBE, in the same cell line. In addition, the single LET value of one ion species gives different outcomes, RBE, for each cell line. LET gives a quantitative description of the radiation quality of the beam and its increase towards the end of the primary particle range represents the main advantage of ion beams. Good predictions of spatial LET distributions in tissues are therefore of crucial importance for the study of radiobiological parameters and, finally, in the treatment planning for hadrontherapy both with protons and light ion beams. Although the single RBE value of 1.1 is currently used in the clinical proton therapy treatments, a number of radiobiological studies have demonstrated considerable variation of RBE. Some of them gave also an overview in the matter (Bettega *et al* 2000, Petrovic *et al* 2010). It was shown that the proton RBE values increased along the spread-out Bragg peaks (SOBP), and that there was a further increase at the distal declining part of the clinical SOBP. Close values were obtained by analyses using Monte Carlo (MC) proton transport simulations (Paganetti and Schmitz 1996, Paganetti 1998, 2002). Higher values of RBE as a function of LET were also measured using low energy protons (Belli *et al* 1998, 2000). Since LET depends on particle species, as well as on its energy, heavier particles have higher energy loss per unit length. Therefore carbon ions reach even higher RBE values than protons, thus improving radiotherapy, particularly for radio-resistant tumours (Weyrather *et al* 1999, 2004, Belli *et al* 2008, Ristic Fira *et al* 2011, Petrovic *et al* 2012). In particular for carbon ion beams, an accurate spatial distribution of RBE is necessary to correctly weight the dose with the biological response (Scholz and Elsasser 2007).

For mono-energetic beams, LET values are easily obtained from tables, but in the case of clinical beams calculations of averaged LET distributions are necessary in order to obtain realistic predictions. Several studies have been carried out in this field and analytical algorithms were developed for this purpose (Wilkens and Oelfke 2002, Kempe *et al* 2007, Grassberger

et al 2011). In most of them certain limitations are still present due the fact that they do not take into account contribution of secondary particles produced by nuclear interactions of primary particles with the target nuclei. This issue can influence the average LET calculations at different depths, in particular when the stopping powers of secondary particles have a larger weight. A more precise tool, able to reproduce in a realistic way the physical interaction of the primary beam with the traversed tissues, is therefore required for this kind of computation. Most of the approaches for RBE modelling are based on analytical LET models that consider primary protons only (Wilkens and Oelfke 2004). Moreover, the majority of the radiobiological experiments performed to study the relation between LET and RBE refer to the incident particle LET, again neglecting the contribution of secondary particles (Matsuura *et al* 2010).

In this paper, a study of LET distributions for protons and carbon ions is carried out with the use of MC methods. A MC application has been developed to simulate usual experimental environment, where depth dose distributions were measured. The developed application allows the computation of the average LET distributions, also taking into account the secondary contributions that are due to nuclear interactions. The main aim of this work is to compute and analyse average LET distributions for hadrontherapy purposes, considering the proton and carbon ions incident beams. The specific tasks of this paper are to:

- simulate dose, fluence and LET distributions for the two transport beam lines that are used at Laboratori Nazionali del Sud (LNS) of the Istituto Nazionale di Fisica Nucleare (INFN) in Catania, currently involved in proton treatments and radiobiological experiments;
- investigate the contribution of the secondary particles in the computation of the average LET, both for protons and carbon ions;
- estimate the difference between the primary and total average LET as a function of depth and show the distinct influence of the secondary contributions of the proton and carbon ion incident beams.

2. Materials and methods

2.1. Dose and track averaged linear energy transfer

All LET definitions that can be found in literature are based on stopping power values. The stopping power is generally expressed as a sum of different and independent components: the electronic (or collision) stopping power due to the collisions of the incident ions with the electrons of the traversed material, the nuclear stopping power, due to the interactions with the nuclei and the radiative stopping power, related to the emission of bremsstrahlung radiation in the electric field of atomic nuclei or atomic electrons (ICRU 1993, 1998). Considering that the last term can be neglected for non-relativistic ion beams and that within this regime the energy transfers are mainly dominated by electronic collisions, the total stopping power is practically reduced to the electronic stopping power. LET in ICRU60 is defined as the restricted linear electronic stopping power, L_Δ, given as:

$$L_\Delta = \frac{\mathrm{d}E_\Delta}{\mathrm{d}l} \tag{1}$$

where $\mathrm{d}E_\Delta$ is the energy lost by a charged particle due to electronic collisions, with the energy transfer less than the specified value Δ, while traversing the distance $\mathrm{d}l$.

If all possible energy transfers are included ($\Delta = \infty$), the LET value coincides with the electronic stopping power (S_{el}) and it is referred as the unrestricted LET (L_∞):

$$L_\infty = S_{\mathrm{el}}. \tag{2}$$

In the case of monochromatic beams, the LET calculation is easily achieved because the kinetic energy is well defined. Different considerations are needed for a non mono-energetic, clinical beam. In this case, the calculation of L_∞ shows additional complexity (Wilkens and Oelfke 2002). At a given depth in tissue, the clinical ion beam has kinetic energy spectrum with different components. Under these conditions it is more meaningful to introduce the concept of LET distribution and hence, to deal with the mean LET value. It represents the local mean of the stopping power S and may simply be referred to the generic term of LET.

Therefore, the defined LET is obtained by averaging, at a given depth z, the particles' stopping powers $S(E)$ where E is the particle energy spectra at z. There are two common definitions of the mean LET: the track averaged LET (L_t) or simply LET-track and the dose averaged LET (L_d) or LET-dose (ICRU 1970, Berger 1993). The first one is the value $S(E)$ weighted by the particle fluence, while the second one is weighted by the local dose. If we now consider the specific particle j, the LET-track can be defined, at the depth z, using the integral notation reported in ICRU16. By slightly modifying its formalism we obtain:

$$L_t^j(z) = \frac{\int_0^\infty S_{\mathrm{el}}^j(E)\varphi_E^j(z)\,\mathrm{d}E}{\int_0^\infty \varphi_E^j(z)\,\mathrm{d}E} \tag{3}$$

where $\varphi_E^j(z)$ is the local particle spectrum of the particle j at the depth z and $S_{\mathrm{el}}^j(E)$ represents the electronic stopping power of the same particle at the energy E.

Similarly, for the LET-dose we have:

$$L_d^j(z) = \frac{\int_0^\infty S_{\mathrm{el}}^{j^2}(E)\varphi_E^j(z)\,\mathrm{d}E}{\int_0^\infty \varphi_E^j(z)\,\mathrm{d}E}. \tag{4}$$

The two kinds of averaged LET calculation can be done for primary particles as well as for each type of secondary particle that is eventually generated in the nuclear interactions of primary particles with the nuclei of the traversed medium. In such a way LET-dose and track for each specific isotope j can be calculated.

On the other hand, it could be of interest to derive a unique value of both LET-track and LET-dose, which takes into account all the different LET contributions ($L_t^j(z)$, $L_d^j(z)$) due to the produced isotopes. This leads to the total LET that can be obtained by averaging the contributions of LET coming from the primary beam as well as from different secondary isotopes calculated with equations (3) and (4) (Wilkens and Oelfke 2002, Kempe *et al* 2007, Seltzer 1993).

This total LET can also be expressed as the total LET-track and the total LET-dose with two analytical expressions similar to equations (3) and (4):

$$\bar{L}_t(z) = \frac{\Sigma_{j=1}^n \int_0^\infty S_{\mathrm{el}}^j(E)\varphi_E^j(z)\,\mathrm{d}E}{\Sigma_{j=1}^n \int_0^\infty \varphi_E^j(z)\,\mathrm{d}E} \tag{5}$$

$$\bar{L}_d(z) = \frac{\Sigma_{j=1}^n \int_0^\infty S_{\mathrm{el}}^{j^2}(E)\varphi_E^j(z)\,\mathrm{d}E}{\Sigma_{j=1}^n \int_0^\infty \varphi_E^j(z)\,\mathrm{d}E}. \tag{6}$$

Here the sum of the j index expresses that the calculation is extended to each kind of j particle that is produced ($j = 1, \ldots, n$).

2.2. The Geant4 hadrontherapy application

Hadrontherapy is a free and open source application developed, regularly maintained and released inside the official GEANT4 (GEometry ANd Tracking) distribution among the

advanced examples. GEANT4 is a code developed in C++ with object-oriented techniques, devoted to the transport of particles in matter (Agostinelli *et al* 2003). It is not a stand-alone MC executable, but a toolkit organized into categories of classes. Initially developed for high energy physics experiments, it is intensively used for medical applications for several years, allowing the tracking of any charged and uncharged particle relevant for radiation therapy. The GEANT4 toolkit is capable of simulating a comprehensive range of physical processes, including electromagnetic, hadronic and optical processes. It includes methods that provide basic functions for simulations, handling set-up geometry, tracking primary and secondary particles and calculating their energy deposition in matter (Allison *et al* 2006). During last years a big effort has been made in order to validate the physics models in the energy range of interest for medical physics, particularly for proton therapy (Jiang and Paganetti 2004) and for therapy with electrons and photons (Carrier *et al* 2004, Larsson *et al* 2005).

The hadrontherapy example has the aim to study issues related to hadrontherapy with protons and light ion beams as well as to provide users with the tool for general-purpose investigations in this field. It was initially developed for the simulation of the CATANA (Centro di AdroTerapia ed Applicazioni Nucleari Avanzate) beam line of the LNS—INFN in Catania, where ocular tumours are treated using the 62 MeV proton beams accelerated by the superconducting cyclotron (Cirrone *et al* 2004, Cuttone *et al* 2011). Hadrontherapy permits the simulation, via simple macro commands, of a beam line for proton/ion therapy including all the necessary transport elements: diffusion and modulation systems for spatial and energy distribution of particles, collimators, transmission detectors, as well as detectors for dose distribution measurements (Cirrone *et al* 2005). In the last version, hadrontherapy provides improved capabilities in the definition of the geometrical setup and physics models (Cirrone *et al* 2011). Specific tools were added to permit simple switch between different geometrical setups (while leaving unchanged the detection system) and to allow clear and error-free activation of the available physics models (Romano *et al* 2011). Exploiting the power of these new features, both the proton and carbon experimental beam lines of LNS–INFN, commonly used for radiobiological experiments, were simulated using the same simulation environment. This procedure guarantees the best quality of the obtained final results: the use of the same application in the two cases permits minimization of the code-related errors and high level of homogeneity and consistency of the attained results.

State-of-the-art of the physics models available inside the GEANT4 framework were used to produce all the presented results. The QGSP_BIC_EMY Reference Physics List was used. It was specifically created to address simulation problems for which high level of accuracy is required, as it is the case in medical applications. When this Reference Physics List is activated, the G4EmStandardPhysics_option3 is employed to manage the electromagnetic processes. The Binary Cascade model is adopted for the nucleus–nucleus inelastic interactions. The QGSP_BIC_EMY also activates models for the decay physics and for the hadronic elastic processes.

The average LET distributions presented in this work have been achieved using the Geant4.9.6.p02 version of the toolkit and the models of the proton and carbon experimental beam lines of INFN–LNS. They are now included in the last release of the hadrontherapy example (Cirrone *et al* 2011, Romano *et al* 2011). Protons and carbon ions that are accelerated by the superconducting cyclotron up to 62 MeV/n, travel in vacuum along the appropriate pipelines and reach after about 80 m the CATANA room or the 0° room, respectively. The first one is used for proton therapy of eye melanoma and for experiments with proton beams, while the second one is used for ion beam measurements and for radiobiological experiments with carbon ions. In both cases the beam exits in air through the 50 μm kapton window. Just before the exit window in vacuum, the first scattering foil made of 15 μm tantalum is placed,

with the tasks of spreading the beam and on-line monitoring the beam current. Proton and carbon ion transport beam lines are identical except for the length in-air (1.8 m for the carbon ion beam line and 2.8 m for the proton one). Also the box hosting energy range shifters and energy modulators is present only in the CATANA beam line. Range shifters and modulators are plastic passive elements adopted in the proton clinical practice to adjust the maximum proton energy and/or its distribution, according to the patient specific tumour location and thickness (Cirrone *et al* 2004). Along the transport in air particles pass through two steel and two plastic collimators and the 50 cm long brass tube ending with the aperture of 25 mm in diameter. They are kept fixed during the whole measurement campaign. The plastic collimators eliminate the particles with large scattering angle and provide the shield from the produced secondary neutrons. The brass tube enables the final beam collimation and creates beams with negligible divergence at the irradiation point. There the beams have circular spot size and flat fluence distribution. A set of two transmission free-air ionization chambers positioned along the transport beam lines, upstream the final brass collimator, provide full control of proton and carbon beam doses during irradiations. The two chambers are independently calibrated with respect to the absolute Markus type ionization chamber, following the recommended procedures of the International Atomic Energy Agency (IAEA) TRS-398 (IAEA 2000). A detailed description of the dosimetric procedures adopted at the LNS irradiation beam lines, can be found elsewhere (Cuttone *et al* 2011).

In this work, the two mentioned beam lines have been simulated inside hadrontherapy and each element has been realistically represented. In order to closely reproduce the experimental depth dose distributions, a PMMA (PolyMethylMethAchrilate) phantom, corresponding to the so-called sensitive detector, was simulated. It was divided into slabs, orthogonal to the beam axis. The slabs were of 100 μm and 10 μm in thickness for the proton and carbon ion cases, respectively. The dose deposited by both primary and secondary particles was collected at the end of the simulation in each slab. Fluence, kinetic energy spectra and average LET distributions were retrieved at the same depths, as described in the following section. A similar approach can be used considering voxels division instead of slabs. As regards the primary beam characteristics, the Gaussian energy distribution was used, centred at the nominal energy of 62 MeV/n and with an energy spread of 0.1%. The Gaussian spatial distribution with a FWHM (full width at half maximum) of 6 mm has been considered and the beam initial momentum was set parallel to the beam line direction.

2.3. LET implementation within the hadrontherapy application

The class for LET calculations has been implemented inside the hadrontherapy application. As described in section 2.2., both electromagnetic and nuclear processes were implemented in the simulation. Therefore secondary particles produced in nuclear interactions were also taken into account. The contribution of secondary charged particles to the mean LET has distinct influences for protons and carbon ion beams, depending also on the specific depth regions. In both cases a mixed radiation field is created and different secondary contributions to the averaged LET distributions have to be combined together.

In section 2.1. two different mean LET definitions were treated: the track averaged LET (LET-track) and the dose averaged LET (LET-dose). A reasonable choice has to be done when such kind of computations have to be linked to radiobiological studies and when cross-comparisons must be carried out for different incident beam configurations. In this work, where the protons and carbon ions incident beams are considered, the LET-dose was used. Even though LET-track may be more meaningful when dealing with high-LET ions, due to the small number of tracks for sub-cellular targets, LET-dose could be more directly related

to the expected biological response. Indeed, when RBE distributions have to be provided by clinical MC calculations, dose averaged parameters are usually evaluated to provide cell survival fraction after irradiations with mixed fields of different LET (Mairani *et al* 2010). In particular α and β parameters of the linear quadratic model are weighted by dose in the step-by-step MC procedure and calculated in the specific point including the contributions of secondary particles.

The initial approach that was adopted for the LET-dose computation made use of the information retrieved step-by-step by the simulation and stored at the end of run for each specific isotope. The used stopping power values were published in tables (ICRU 1993). Wilkens *et al* employed a similar approach, but they only included primary and secondary protons (Wilkens and Oelfke 2002). When considering the specific isotope j, the procedure that was implemented consists of registering and scoring the kinetic energies of the particles j when they traverse the specific slab located at the depth position z inside the PMMA phantom. Due to interactions suffered along the path, the beam traversing medium is not mono-energetic. Therefore, a local spectrum is present for each depth z, characterized by an energy spread, which increases with the depth z. In the Geant4 hadrontherapy application we simulated this complex configuration and calculated the LET-dose following the definitions given in the equations (5) and (6). For each particle j an accurate estimation of the local spectrum of kinetic energy is needed, which is stored in histograms. An energy bin of 250 KeV was chosen for the energy spectra, together with the energy threshold of 250 KeV. Once the local energy spectra are collected for each particle and depth, they have to be coupled with the corresponding stopping power values in order to obtain the average LET. If $\phi_{i,j}(z)$ indicates the number of j particles in the energy bin i ($i = 1, \ldots, N$) and $S_{i,j}$ indicates the stopping power corresponding to the same energy bin for the specific j isotope, thus the LET-dose was computed as follows:

$$\bar{L}_d^{MC}(z) = \frac{\Sigma_{j=1}^{K}\Sigma_{i=1}^{N}\varphi_{i,j}(z)S_{i,j}^2}{\Sigma_{j=1}^{K}\Sigma_{i=1}^{N}\varphi_{i,j}(z)S_{i,j}} \tag{7}$$

where the index $j = 1,\ldots, K$ indicates the specific charged isotope created at the end of the simulation. The stopping power values $S_{i,j}$, used in equation (7), were retrieved in tables (ICRU 1993), using ad hoc methods that allow point interpolations when the required value is not available. Equation (7) represents the discrete version of equation (6), and it has been directly implemented inside the hadrontherapy application. Thus, at the end of the simulation run, the depth distribution of the LET-dose is obtained for each single isotope j as well as for the total contribution due to all the isotopes present in the mixed radiation field.

A different approach was implemented in the final version of the MC application and it was compared with the previous one. In this second approach the final average LET is computed in an easier and more realistic way. Indeed, at a specific depth z, LET is averaged step-by-step without explicitly separating the contributions due to different isotopes: their contributions are directly included as well as those of the primary particle, because stopping power is calculated on flight for each step done by the specific particle. Fixing the specific depth z, energy deposited along the step $\mathrm{d}E$ is divided by the particle step length ds and the stopping power calculated for the specific step is weighted by the released energy in the step:

$$\bar{L}_d^{MC}(z) = \frac{\Sigma_{k=1}^{M}\mathrm{d}E_k(\mathrm{d}E_k/\mathrm{d}x_k)}{\Sigma_{k=1}^{M}\mathrm{d}E_k} \tag{8}$$

where $k = 1, \ldots, M$ represents the steps done by both primary and secondary particles in the fixed slab z. This method has been finally used for the simulations, because it calculates the

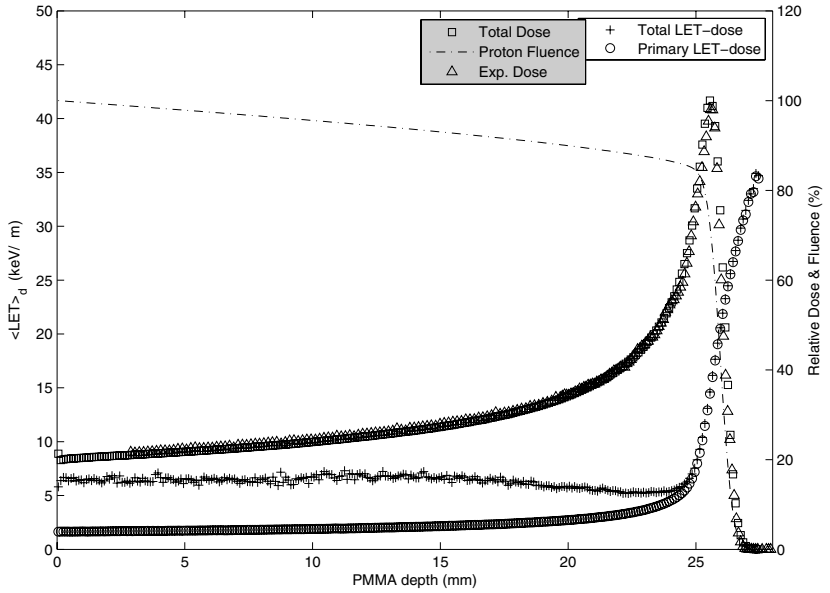

Figure 1. Total and primary LET-dose distributions for the proton beam of 62 MeV in PMMA, obtained with the Geant4 simulations. Relative dose distributions and primary protons fluence are given in arbitrary units. Dose is compared with experimental data, normalized at the entrance.

local stopping power without using pre-defined tables and avoids the approximation of binning storage. Moreover, lower memory usage characterizes this approach, since no energy spectrum per isotope is computed and stored but just the energy deposited per step is registered. Each produced particle was tracked down to zero kinetic energy. Only the production cut off for secondary electrons, positrons and gammas were implemented and they were set to 0.01 mm. A total of 10^7 primary events were simulated.

3. Results

The LET-dose was calculated for two different experimental transport beam lines: on for the 62 MeV protons and 62 MeV/n carbon ion beams, available at INFN–LNS in Catania and described in section 2.2. For both protons and carbon ions, two different beam configurations were considered: the mono-energetic and the spread-out. For each specific configuration dose, fluence, primary and total LET-dose were computed. In the same plots, the comparison with the experimental depth dose distributions are also shown. These data were acquired by the air ionization Markus chamber with the spatial distribution ranging between 10 and 100 μm. The impact of the secondary particles on the total average LET-dose was investigated for each specific configuration and its influence on the final results was shown comparing the total and primary LET-dose. The depth dependence of LET was computed in PMMA, as this material is mainly used in radiobiological experiments during cell irradiations. Flasks containing cell samples and slabs that are inserted in front of them in order to simulate the desired depth in tissue (position along the Bragg curve) are usually made of this material. All the results that are presented in this work were also obtained in water as reference with other published results.

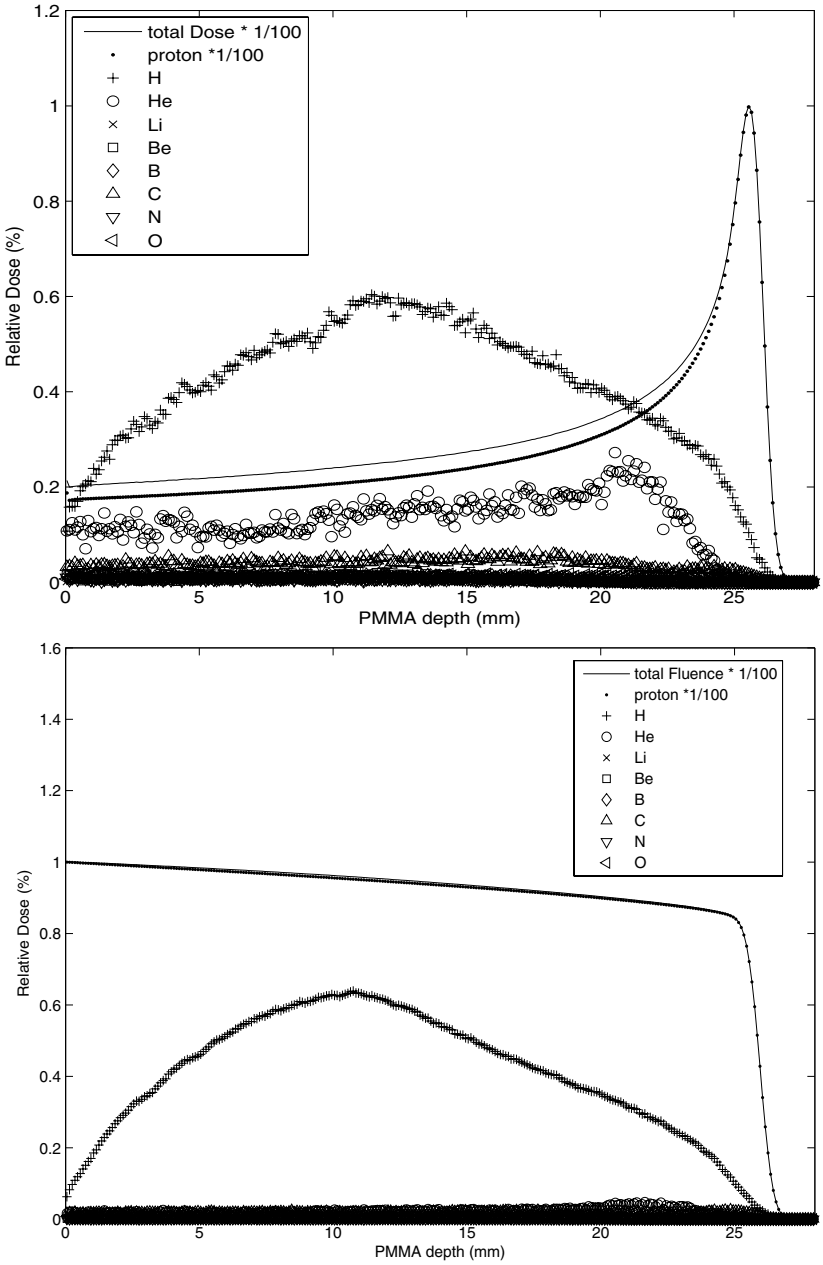

Figure 2. Contributions of the secondary particles in terms of dose (top) and fluence (bottom) for pristine proton beam of 62 MeV in PMMA, obtained with Geant4. Depth dose distributions for the total and proton dose/fluence are scaled by the factor 10.

3.1. LET for the 62 MeV proton beams

Proton beams with the initial energy of 62 MeV, that is usually applied for the eye melanoma therapy, were analysed. Even though mono-energetic beams are not clinically used, we firstly

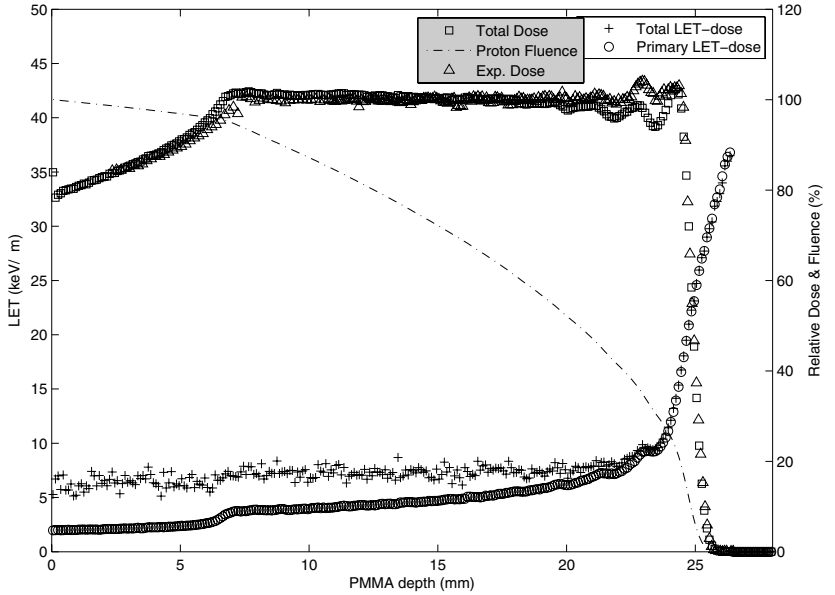

Figure 3. Total and primary LET-dose distributions for the spread-out Bragg peak in PMMA, obtained with the Geant4 simulation. Relative dose distributions and primary protons fluence are given in arbitrary units. Dose is compared with experimental data, normalized at the centre of the modulated region.

investigated this configuration in order to focalize on a more simple configuration and to study the LET dependence for the fixed energy. In the following section the SOBP, used for clinical ocular treatment, will be analysed. Figure 1 shows the depth dependence in PMMA of primary and total LET-dose for the 62 MeV pristine proton beams. A range in PMMA of 25.5 mm was found with a peak–plateau ratio of 5. In the same plot, the primary proton fluence and total released dose are also given. The depth dose is compared with experimental data acquired at LNS.

A good agreement between the experimental dose distribution and results obtained with the Geant4 simulations was found. Due to nuclear interactions of protons with target nuclei, the primary fluence reduces to 85% in proximity of the Bragg peak and then steeply falls down in 0.15 mm, where the highest LET values are achieved. In the entrance region of the beam LET slowly increases and rapidly grows up towards the protons range. LET-dose values, considering only primary protons (primary LET-dose) or the total contribution of both primary and secondary particles (total LET-dose) have a common trend in proximity of the range, where they both reach a maximum value of 37 KeV μm^{-1}. Different values for primary and total LET-dose were found in the entrance channel. In the first 20 mm of depth, the primary mean LET ranges between 1.5 and 2.5 KeV μm^{-1}, whereas the total mean LET ranges between 6 and 7 KeV μm^{-1}. This difference is due to high-LET contributions coming from the secondary ions produced in non-elastic nuclear interactions. Switching off the nuclear processes in the MC simulation, no difference is found between the two distributions. A large variety of isotopes are produced because of elastic and non-elastic nuclear interactions of the primary protons with the target nuclei. In figure 2 the contribution of the secondary particles in terms of dose and fluence is shown. There is a major contribution of the secondary protons and a non-negligible contribution from alpha particles. However, the secondary dose and fluence

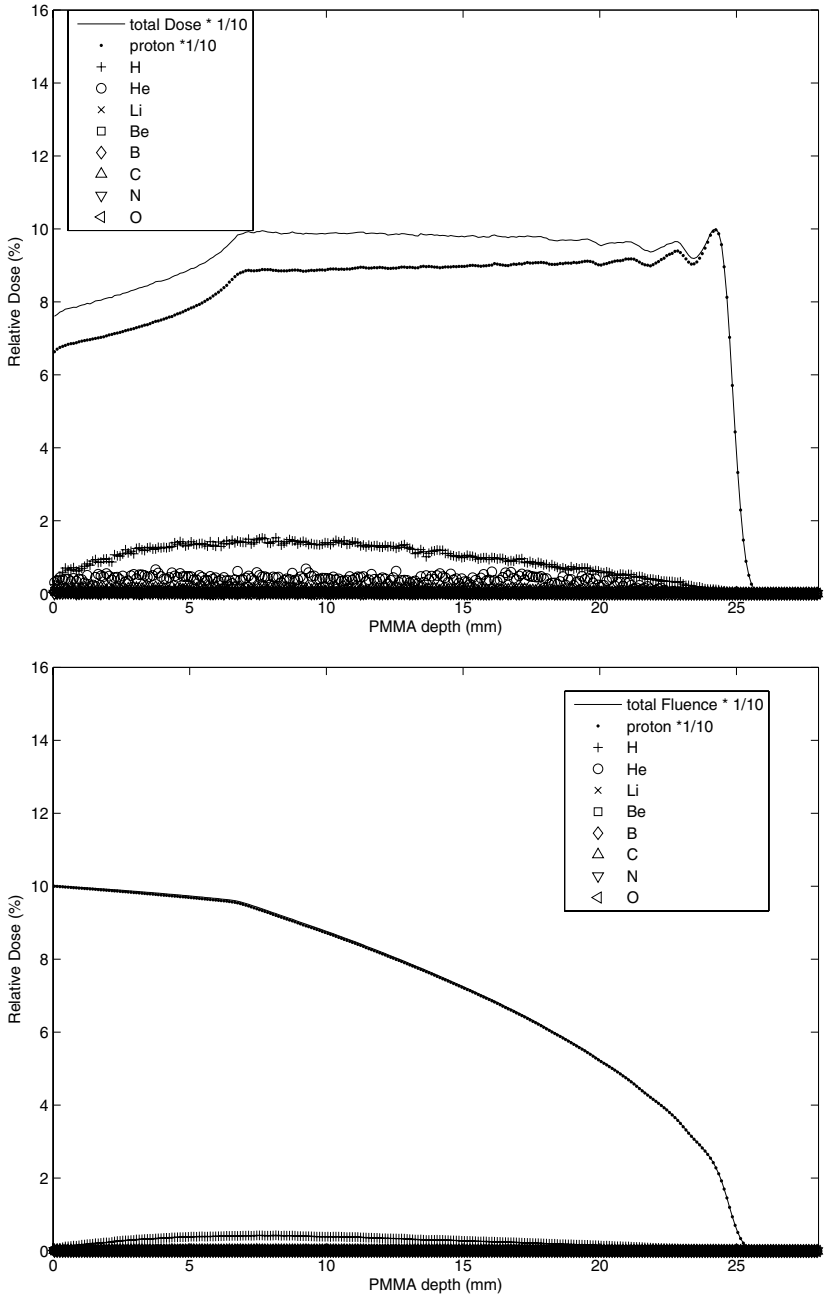

Figure 4. Contributions of the secondary particles in terms of dose (top) and fluence (bottom) for SOBP proton beam of 62 MeV in PMMA, obtained with Geant4. Depth dose distributions for the total and proton dose/fluence are scaled by the factor 10.

alone cannot explain the difference in primary and total LET-dose, because the local energy spectra have the main role in such computation. How to assess this contribution is discussed in section 4.

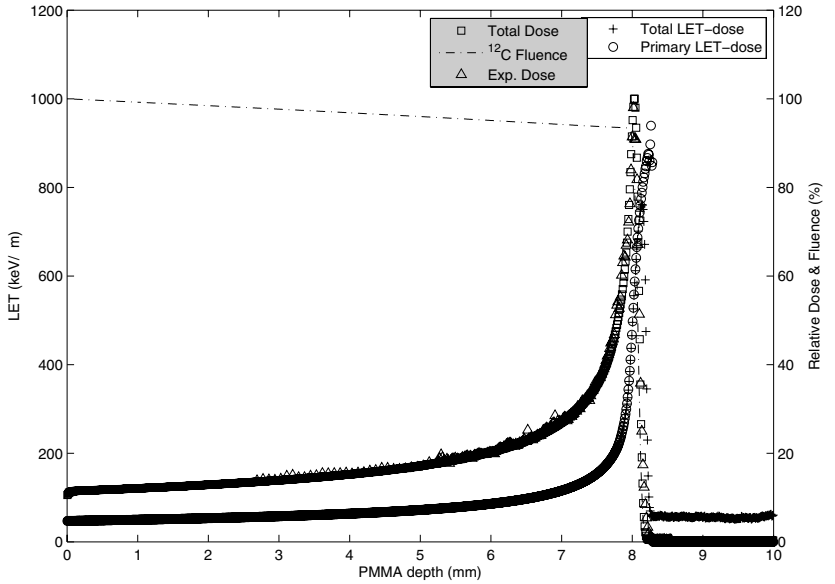

Figure 5. Total and primary LET-dose distributions for the carbon ion beam of 62 MeV/n in PMMA, obtained with the Geant4 simulations. Relative dose distributions and primary carbon fluence are given in arbitrary units. Dose is compared with experimental data, normalized at the entrance.

3.2. LET for the spread-out proton Bragg peak (SOBP)

A more realistic configuration has been also considered by incorporating in the MC simulation one of the modulation wheels that is frequently used in the ocular proton treatments of the CATANA facility (Cirrone *et al* 2004, Cuttone *et al* 2011). The combination of the wheel and range-shifter chosen for this work is able to passively shape the beam within the modulation region of 18 mm in PMMA (95% proximal to 95% distal dose), which is one of the most common in the clinical practice. The comparison between the simulated and experimental depth dose distributions is shown in figure 3, together with the LET calculations. Some discrepancies are found in this case in the dose comparison: they may reach 5% in the final part of the peak. This can be due to small defects in the wheel construction, which were not reproduced in the MC simulation. In fact, minor differences in the thickness of the last (and thinnest) wheel steps, may produce a slightly negative influence in particular at the end of the peak where LET increases.

Primary fluence gradually decreases, due to the ranges that correspond to each specific single peak, varying from 96% to 16% along the modulation region. As in the previous case of the mono-energetic beam, the primary and total LET-dose show a common trend in the distal part of the peak where the same maximum value of the pristine peak configuration is reached. The discrepancy that is obtained in the entrance channel is again due to the effects of secondary heavy ions, as already discussed in the previous section. In addition fluctuations are more evident due to the proton scattering in the range-shifter and modulator wheel, which considerably reduces the total primary fluence. At the beginning of the modulation region, there is an increase of the mean LET and it corresponds to the beginning of the SOBP. Along the modulation region the primary LET gradually grows up ranging between 3 and 18 KeV μm^{-1}. The LET increase is less pronounced for the total LET, where the secondary ion

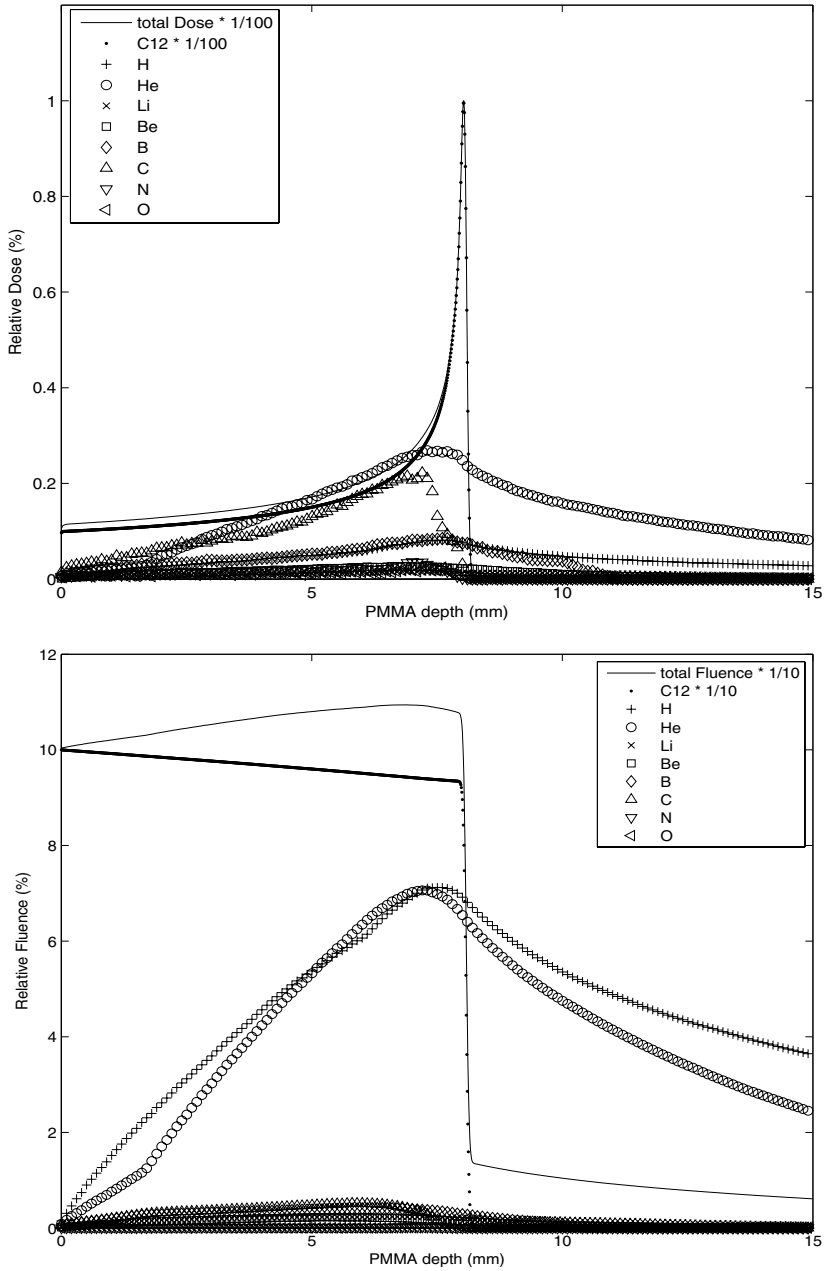

Figure 6. Contributions of the secondary particles in terms of dose (top) and fluence (bottom) for the pristine carbon beam of 62 MeV/n in PMMA, obtained with Geant4. Depth dose distributions for the total and carbon dose are scaled by the factor 100, for total and carbon fluence by the factor 10.

contributions somewhat cover the rise of the primary stopping power. Similar results as in the case of the pristine peak were found for the secondary particle dose and fluence and are shown in figure 4.

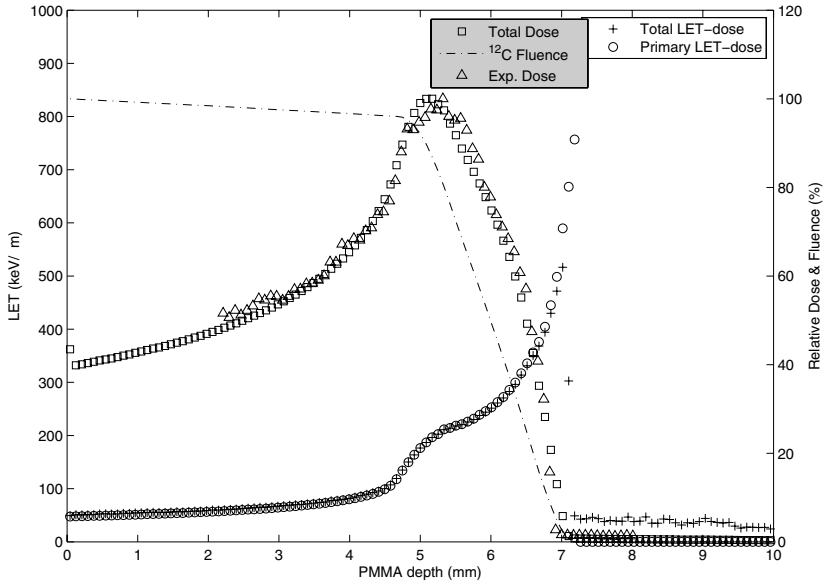

Figure 7. Total and primary LET-dose distributions for the spread-out carbon Bragg peak in PMMA, obtained with the Geant4 simulations. Relative dose distributions and primary carbon ions fluence are given in arbitrary units. Dose is compared with experimental data, normalized at the entrance.

3.3. LET for the 62 MeV/n carbon ion beams

The results obtained with the carbon ion incident beams are shown in the present and in the following section. These beams are of great interest because of their higher biological efficiency. Various radiobiological experiments are performed world wide with such a kind of beams. At LNS a large number of cell irradiations measurements were carried out with the 62 MeV/n carbon ions. This is the reason why this energy was chosen as the reference energy for the LET depth dependence analysis (Belli *et al* 2008, Ristic Fira *et al* 2011, Petrovic *et al* 2012, Koricanac *et al* 2013).

Again the pristine Bragg peak configuration, characterized by the mono-energetic carbon beam, was the first to be considered. Subsequently a more realistic case in which a passive element is used for spreading the peak will be considered. As mentioned in section 2.2, the experimental transport beam line was fully simulated, in order to accurately take into account the energy loss in air and along the traversed passive elements. To compare Geant4 results with the acquired data the experimental depth dose distributions were obtained with the same experimental procedure that was mentioned before. According to figure 5, there is a good agreement between the two distributions, characterized by the peak–plateau ratio that is about two times higher respect to the proton case. The primary and total mean LET values reach much higher levels with respect to protons. They also show a completely different relative trend regarding protons. Figure 5 shows that the primary and total LET-dose have the same values both in the entrance channel and in the proximal part of the peak. Only in the distal part of the peak and in the tail they show a different trend. In the entrance channel they are characterized by the common LET value of 48 KeV μm^{-1}, while in the last part of the peak primary LET-dose reaches the maximum value of 750 KeV μm^{-1} and the total LET-dose the maximum value of 870 KeV μm^{-1}. In the tail beyond the peak the primary LET-dose steeply drops and the total LET-dose has the initial value of about 55 KeV μm^{-1}.

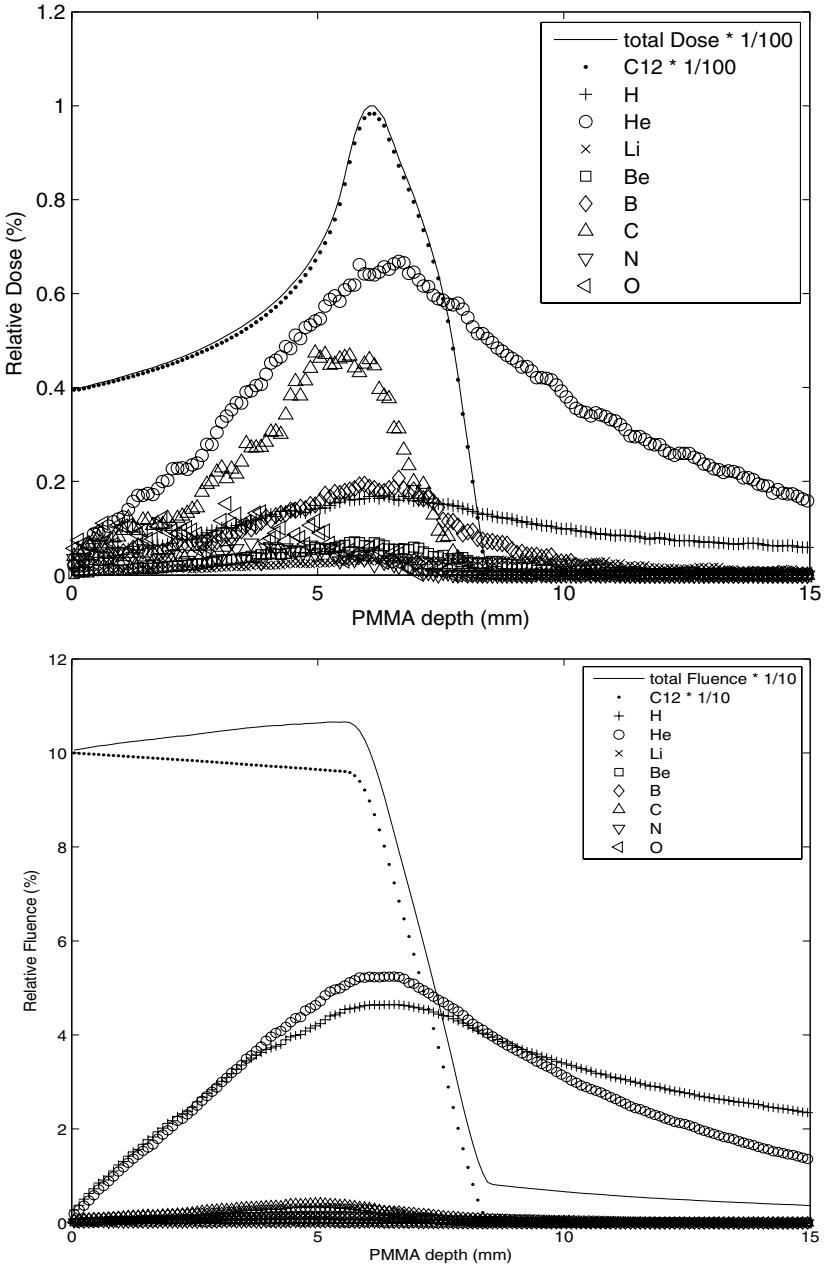

Figure 8. Contributions of the secondary particles in terms of dose (top) and fluence (bottom) for the spread-out carbon beam of 62 MeV/n in PMMA, obtained with Geant4. Depth dose distributions for the total and carbon dose are scaled by the factor 100, for total and carbon fluence by the factor 10.

These results can be explained considering again the influence of non-elastic nuclear interactions of the primary particles with the target nuclei. In the case of the carbon ion incident beams, the contribution of the secondary particles to the total LET-dose is mainly due to projectile fragments, which are characterized by larger range. This is obvious in figure 6,

where in particular the secondary protons and alphas, created along the primary carbon path, deliver their dose far beyond the Bragg peak position. Therefore, as discussed more in detail in section 4, their contribution, although relatively small, mainly influences the tail after the peak.

3.4. LET for the carbon ion spread-out Bragg peak

Similar results have been obtained for the carbon ion spread-out peak. In this case, the ripple-filter passive element was used for degrading the beam and obtaining a slightly larger Bragg peak. It is a PMMA device with a segmented central area that is traversed by the beam (Bourhaleb *et al* 2008). Two ripple-filters specifically designed for the 62 MeV/n carbon ion beams were incorporated in the MC computation. They are widely used at INFN–LNS for radiobiological experiments with the carbon ions. The configuration including two ripple-filters at the relative distance of 10 cm was adopted in order to achieve further enlargement of the peak. This is the reference configuration that is used in the mentioned cell samples irradiations.

Experimental data, shown in figure 7, were acquired with the already described procedures and compared with Geant4 results. The fluence and primary/total average LET are also shown in the same figure. Considering the wider peak, a more gradual fluence decreasing is found. For the primary and total LET-dose, the same considerations as before are valid also in this case. The only difference can be found in the trend of LET depth distribution. This is due to the presence of the two ripple-filters that degrade and enlarge the beam. Again, as shown in figure 8, the contribution of the secondary particles mainly influences the distal part.

4. Discussion and conclusions

The presented Geant4-based tool is able to calculate the primary and total LET-dose for all kinds of geometrical configurations and incident beams. For the incident beams considered in this work, the increase of LET towards the end of range is more pronounced for the pristine Bragg peaks than for the SOBP. Such behaviour was also pointed out by other authors (Wilkens and Oelfke 2002, Kempe *et al* 2007).

It is clear from the present study that the contribution of the secondary particles due to non-elastic nuclear interactions influences the distribution of the total LET-dose. For the incident proton beams, some investigations have been done in order to understand how to take into account these contributions for biological assessments. So far it is not clear how to include in particular the contribution from heavy secondary particles (Grassberger *et al* 2011, Berger 1993). In these studies, both analytical and MC approach were used to take into account the secondary contributions for the average LET computations. The dose averaged LET distributions for the pristine Bragg peak and SOBP have been computed by Wilkens and Oelfke, who also developed a fast analytical model for the prediction of LET distributions in water phantoms (Wilkens and Oelfke 2002). In their work, the secondary particles due to non-elastic nuclear interactions are not fully taken into account. They only consider the contribution of the secondary protons neglecting the production of light and heavy ions. In order to crosscheck the Geant4 LET-dose computations, we compared our results with those obtained by Wilkens and Oelfke for the pristine proton peaks at 70 and 150 MeV. The same configuration was simulated, including the same parameters for the initial energy spread. It was considered that only the secondary protons contribute to the total LET-dose. Our data agree well with their results with the maximum discrepancy of 0.5 KeV μm^{-1} for the LET-dose in the entrance region (about 0.5 KeV μm^{-1} at 160 MeV and

1 KeV μm^{-1} at 70 MeV). If we include the secondary particle contributions large deviations are found for the total LET-dose, which is due to the presence of the secondary particles. Initial investigations with this aim were done in the way that the LET-dose distributions were calculated using the MC approach (Berger 1993, Seltzer 1993). In these works separate curves for the primary protons only and for the primary and secondary particles were acquired, obtaining large differences in the LET-dose distributions, especially in the entrance channel. Grassberger *et al* have used a similar approach, but they only considered the contribution of the primary and secondary protons, electrons and photons, neglecting light ions (Grassberger *et al* 2011).

In the present study similar results to those of Seltzer were obtained for proton beams and are shown in sections 3.1 and 3.2. For the pristine proton Bragg peak in the entrance channel the total LET-dose is roughly a factor of 4 higher than the primary one (figure 1). We specifically investigated the source of the high-LET contribution by including separately in the total LET computation the weights due to the specific ions. The largest contribution was estimated to be due to carbon and oxygen ions produced by non-elastic nuclear interactions of protons with the target. Following the nuclear de-excitation, the low energy residual nuclei are produced. They are characterized by a very high LET, with respect to the stopping power of protons at the same specific depth. Even though the production cross sections of the mentioned ions are very low, their contribution in the total LET-dose is quite large. This is caused by the high amount of their local energy deposition in a very short range. For track average LET, where computation is weighted by fluence instead of dose, we found a factor of 2 lower values in the same regions. The contribution of these secondary ions is more pronounced in the entrance region, where the energy is high enough to produce a significant number of non-elastic nuclear interactions. As shown in figure 1, at or behind the Bragg peak, the secondary particles can be neglected. Larger fluctuations are observed in the case of the total LET-dose with respect to the primary one. This is because of low statistics characterizing these low-probability events related to the nuclear interactions.

The high-LET components for the clinical proton beams were recently analysed, considering also contributions from the secondary charged particles (Grassberger and Paganetti 2011). The influence of the secondary particles on the LET-dose distribution was separately studied. It was shown that the secondary protons have a significant impact, leading to an increase in LET-dose up to the factor of 10 for the same depth. Also, the contributions from alpha particles and heavier ions was analysed, concluding that even though alpha particles surely inflict biological damage, the situation is less clear for the heavier ions. For instance, in the case of the secondary carbon ions, a negligible percentage of their deposited dose is due to those with the energy able to traverse 10 μm (assuming this as a reasonable cell diameter). The authors also claim that it is not possible to exclude that the low energy carbon ions may be created within the cell nucleus; therefore, their contribution cannot be neglected *a priori* in the computation. In the present study we demonstrated that the contribution of the secondary particles, including heavier ones, slightly increases the average LET-dose distributions in the entrance channel for both the pristine and SOBP proton beams. For the clinical cases, where SOBP are used to treat the target, our results show that it might not be possible to completely neglect the contribution of light and heavy ions in the target area, otherwise an underestimation of the LET-dose might be done. In order to better understand the presented results, cell sample irradiations performed in the same conditions were planned.

A rather different situation with respect to protons occurs in the case of the carbon ion incident beams. A few studies were done for the incident ion beams, where the LET distributions for specific ions of interest in hadrontherapy were analysed, trying to separate the low LET and high-LET regions (Kempe *et al* 2007). However, they did not include the

contribution of the secondary ions produced in nuclear interactions. In the presented work, we compared the primary LET-dose with the total one for the carbon ion incident beams, using the same tools as for protons. We analysed the secondary contributions in order to understand how they may influence the average LET distributions and to point out the difference with respect to the proton case. Because of non-elastic nuclear interactions, several lighter ions are produced, most of them coming from the projectile fragmentation. They are produced at roughly the same velocity of the projectile. Together with the primary beam, they traverse the considered thickness. By passing the primary range they create the tail of extra dose after the Bragg peak. Considering their lower atomic number regarding the primary carbon ions, they give the low LET contribution to the total LET-dose. Moreover, their weight is lower with respect to the primary carbon one because lighter ions release lower amount of dose per slab as compared to carbon ions. For this reason in the proximal part the primary carbon LET has the main weight and is practically equivalent to the total LET-dose. On the opposite, beyond the peak the only contribution to the total average is given by the projectile particles, whose energies imply very large ranges. Even though a relatively low dose characterizes the tail at this energy, it is well known that for higher energies used in the carbon clinical treatments (up to 400 MeV/n), the tail dose may reach not so negligible values. Indeed, as shown in several experimental studies, up to 30% of primary carbon ions at 200 MeV/n and up to 70% at 400 MeV/n undergo fragmentation before they stop in the tissues (Haettner *et al* 2013). The relatively high LET found in this region, due to the contribution of all the secondary particles, can enhance the predicted biological effect, therefore representing a challenge for the healthy tissues just after the peak. A precise tool for the total LET-dose computation would be particularly useful for the investigations of the biological events arising in the healthy tissue, thus exploring the possible secondary tumour induction and reducing the related risks. Phenomenological models for the RBE are developed starting from the LET-dose computations that have to be as more realistic as possible (Wilkens and Oelfke 2004).

The results that were presented and analysed in this study considerably improved understanding and helped in the interpretation of biological effects produced on cells by protons along the clinical SOBP. The opposite behaviour of the fluence and LET-dose along the path of protons and particularly close to the end of range, where the distal fall-off part of the SOBP is located, was fully investigated in view of the biological processes that were produced (Petrovic *et al* 2010). In the case of carbon ions, the physics as well as the biological properties of the events at this specific part of the SOBP and even more at the fragmentation tail have not yet been extensively studied. The result of these studies ought to be directly included in the treatment planning system in order to avoid unexpected hot spots in neighboring vital normal tissues.

The tool for the LET computation has been recently included in the last public version of the hadrontherapy advanced example of the current Geant4 release (version 10.0, December 2013). This tool will be also integrated with a module dedicated to RBE computations: an interface to the most common track structure codes will be developed in order to provide biological dose depth curves for different cell lines.

Acknowledgments

This work was financially supported by Istituto Nazionale di Fisica Nucleare, Laboratori Nazionali del Sud, Italy (MC-INFN experiment). The authors would also like to thank Ministry of Education, Science and Technological Development of Serbia (grants 173046 and 171019) for their financial support.

References

Agostinelli S *et al* 2003 Geant4—A simulation toolkit *Nucl. Instrum. Methods Phys. Res.* A **506** 250

Allison J *et al* 2006 GEANT4: developments and applications *IEEE Trans. Nucl. Sci.* **53** 270–8

Baumert B G, Lomax A J, Miltchev V and Davis J B 2001 A comparison of dose distributions of proton and photon beams in stereotactic conformal radiotherapy of brain lesions *Int. J. Radiat. Oncol. Biol. Phys.* **49** 1439–49

Belli M *et al* 1998 RBE-LET relationships for cell inactivation and mutation induced by low energy protons in v79 cells: further results at the LNL facility *Int. J. Radiat. Biol.* **74** 501–9

Belli M *et al* 2000 Inactivation of human normal and tumour cells irradiated with low energy protons *Int. J. Radiat. Biol.* **76** 831–9

Belli M *et al* 2008 Effectiveness of mono-energetic and spread-out Bragg peak carbon-ions for inactivation of various normal and tumour human cell lines *J. Radiat. Res.* **49** 597–607

Berger M J 1993 Penetration of proton beams through water I. Depth-dose distribution, spectra and LET distribution *NISTIR Technical Report* 5226 (Gaithersburg, MD: National Institute of Standards and Technology)

Bettega D, Calzolari P, Chauvel P, Courdi A, Herault J, Iborra N, Marchesini R, Massariello P, Poli G L and Tallone L 2000 Radiobiological studies on the 65 MeV therapeutic proton beam at Nice using human tumour cells *Int. J. Radiat. Biol.* **76** 1297–303

Bourhaleb F *et al* 2008 Monte Carlo simulations of ripple filters designed for proton and carbon ion beams in hadrontherapy with active scanning technique *J. Phys.: Conf. Ser.* **102** 012002

Brada M, Madelon P J and De Ruysscher D 2007 Proton therapy in clinical practice: current clinical evidence *J. Clin. Oncol.* **25** 965–70

Carrier J F, Archambault L, Beaulieu L and Roy R 2004 Validation of GEANT4, an object-oriented Monte Carlo toolkit, for simulations in medical physics *Med. Phys.* **31** 484–92

Cirrone G A P *et al* 2004 A 62-MeV proton beam for the treatment of ocular melanoma at Laboratori Nazionali del Sud-INFN *IEEE Trans. Nucl. Sci.* **51** 860–5

Cirrone G A P, Cuttone G, Guatelli S, Lo Nigro S, Mascialino B, Pia M G, Raffaele L, Russo G and Sabini M G 2005 Implementation of a new Monte Carlo—GEANT4 simulation tool for the development of a proton therapy beam line and verification of the related dose distributions *IEEE Trans. Nucl. Sci.* **52** 1756–58

Cirrone G A P *et al* 2011 Hadrontherapy: a Geant4-based tool for proton/ion-therapy studies *Prog. Nucl. Sci. Technol.* **2** 207–12

Cuttone G *et al* 2011 CATANA protontherapy facility: the state of art of clinical and dosimetric experience *Eur. Phys. J. Plus* **126** 1–7

Gerweck L E and Kozin S V 1999 Relative biological effectiveness of proton beams in clinical therapy *Radiother. Oncol.* **50** 135–42

Grassberger C and Paganetti H 2011 Elevated LET components in clinical proton beams *Phys. Med. Biol.* **56** 6677–91

Grassberger C, Trofimov A, Lomax A and Paganetti H 2011 Variations in linear energy transfer within clinical proton therapy yields and the potential for biological treatment planning *Int. J. Radiat. Oncol. Biol. Phys.* **80** 1559–66

Haettner E, Iwase H, Kramer M, Kraft G and Schardt D 2013 Experimental study of nuclear fragmentation of 200 and 400 MeV/u 12C ions in water for applications in particle therapy *Phys. Med. Biol.* **58** 8265–79

IAEA 2000 Absorbed dose determination in external beam radiotherapy—an international code of practice for dosimetry based on standards of absorbed dose to water *International Atomic Energy Agency Technical Reports Series* 398

ICRU 1970 Linear energy transfer *International Commission on Radiation Units and Measurements Technical Report* 16 (Washington, DC: ICRU)

ICRU 1993 Stopping powers and ranges for protons and alpha particles *International Commission on Radiation Units and Measurements Technical Report* 49 (Bethesda, MD: ICRU)

ICRU 1998 Fundamental quantities and units for ionizing radiation *International Commission on Radiation Units and Measurements Technical Report* 60 (Bethesda, MD: ICRU)

Jiang H and Paganetti H 2004 Adaptation of GEANT4 to Monte Carlo dose calculations based on CT data *Med. Phys.* **31** 2811–8

Kempe J, Gudowska I and Brahme A 2007 Depth absorbed dose and LET distributions of therapeutic 1H, 4He, 7Li, and 12C beams *Med. Phys.* **34** 183

Koricanac L, Zakula J, Keta O, Cirrone G A P, Cuttone P, Ristic-Fira A and Petrovic I 2013 Carbon ions induce DNA double strand breaks and apoptosis in HTB140 melanoma cells *Nucl. Technol. Radiat. Prot.* **28** 195–203

Kraft G 2000 Tumor therapy with heavy charged particles *Prog. Part. Nucl. Phys.* **45** 473–544

Larsson S, Svensson R, Gudowska I, Ivanchenko V and Brahme A 2005 Radiation transport calculations for 50 MV photon therapy beam using the Monte Carlo code GEANT4 *Radiat. Prot. Dosim.* **115** 503–7

Matsuura T *et al* 2010 Apparent absence of a proton beam dose rate effect and possible differences in RBE between Bragg peak and plateau *Med. Phys.* **37** 5376–81

Mairani A, Brons S, Cerutti F, Fass A, Ferrari A, Kramer M, Parodi K, Scholz M and Sommerer F 2010 The FLUKA Monte Carlo code coupled with the local effect model for biological calculations in carbon ion therapy *Phys. Med. Biol.* **55** 4273–89

Paganetti H and Schmitz Th 1996 The influence of the beam modulation technique on dose and RBE in proton radiation therapy *Phys. Med. Biol.* **41** 1649–63

Paganetti H 1998 Calculation of the spatial variation of relative biological effectiveness in a therapeutic proton field for eye treatment *Phys. Med. Biol.* **43** 2147–57

Paganetti H and Goitein M 2001 Biophysical modelling of proton radiation effects based on amorphous track models *Int. J. Radiat. Biol.* **77** 911–28

Paganetti H and Kooy H 2010 Proton radiation in the management of localized cancer *Expert Rev. Med. Devices* **7** 275–85

Petrovic I, Ristic-Fira A and Todorovic D 2010 Response of a radio-resistant human melanoma cell line along the proton spread-out Bragg peak *Int. J. Radiat. Biol.* **86** 742–51

Petrovic I, Ristic-Fira A, Todorovic D, Koricanac L, Zakula J, Cirrone G A P, Romano F and Cuttone G 2012 Radio-resistant human malignant cells after irradiations with 1H and 12C ions of different LET *Radiother. Oncol.* **102** 108–9

PTCOG, Particle Therapy Cooperative Group 2013 http://ptcog.web.psi.ch/

Ristic-Fira A, Todorovic D, Zakula J, Keta O, Cirrone G A P, Cuttone G and Petrovic I 2011 Cellular response to conventional radiation and hadrons *Physiol. Res.* **60** S129–35

Romano F, Cirrone G A P, Cuttone G, Di Rosa F, Mazzaglia S E, Sabini M G and Sardina D 2011 Applications of Monte Carlo methods to special radiotherapeutic techniques *Nuovo Cimento Soc. Ital. Fis.* C **34** 167–73

Schardt D, Elsasser T and Schulz-Ertner D 2010 Heavy-ion tumor therapy: physical and radiobiological benefits *Rev. Mod. Phys.* **82** 383–425

Scholz M and Elsasser T 2007 Biophysical models in ion beam therapy *Adv. Space Res.* **40** 1381–91

Seltzer S M 1993 An assessment of the role of charged secondaries from nonelastic nuclear interactions by therapy protons beams in water *National Institute of Standards and Technology Publication* 5221 (Gaithersburg, MD: NISTIR)

Wambersie A 1999 RBE, reference RBE and clinical RBE: applications of these concepts in hadron therapy *Strahlenther. Onkol.* **175** 39–43

Weyrather W K, Ritter S, Scholz M and Kraft G 1999 RBE for carbon track-segment irradistio in cell lines of differing repair capacity *Int. J. Radiat. Biol.* **75** 1357–64

Weyrather W K and Kraft G 2004 RBE for carbon ions: experimental data and the strategy of RBE calculation for treatment planning *Radiother. Oncol.* **75** S161–9

Wilkens J and Oelfke U 2002 Analytical linear energy transfer calculations for proton therapy *Med. Phys.* **30** 806

Wilkens J and Oelfke U 2004 A phenomenological model for the relative biological effectiveness in therapeutic proton beams *Phys. Med. Biol.* **49** 2811–25

Wouters B G, Lam G K, Oelfke U, Gardey K, Durand R E and Skarsgard L D 1996 Measurements of relative biological effectiveness of the 70 MeV proton beam at TRIUMF using Chinese hamster v79 cells and the high-precision cell sorter assay *Radiat. Res.* **146** 159–70